Imperfection-sensitive ductility of aluminium thin films

M. Coulombier,[a,b,*] A. Boé,[a,c,d] C. Brugger,[a,b] J.P. Raskin[a,c] and T. Pardoen[a,b]

[a] *Research Center in Micro and Nanoscopic Materials and Electronic Devices (CeRMiN), Université catholique de Louvain, B-1348 Louvain-la-Neuve, Belgium*
[b] *Institute of Mechanics, Materials and Civil Engineering (iMMC), Université catholique de Louvain, B-1348 Louvain-la-Neuve, Belgium*
[c] *Information and Communication Technologies, Electronics and Applied Mathematic (ICTEAM), Université catholique de Louvain, B-1348 Louvain-la-Neuve, Belgium*
[d] *IEMN UMR CNRS8520, IRCICA FR CNRS3024 Université de Lille, 59651 Villeneuve d'Ascq, France*

Received 16 December 2009; revised 25 January 2010; accepted 28 January 2010
Available online 1 February 2010

Ductility, defined as the strain at the onset of necking, has been characterized in thin Al films using an on-chip, internal stress actuated, microtensile testing setup. In the smallest specimens, the ductility is equal to 0.08 and 0.27 for 200 and 375 nm thick films, respectively, while the average strain-hardening exponents are, respectively, equal to 0.11 and 0.23. In addition to the thickness effect, ductility decreases with increasing specimen size due to imperfection sensitivity, involving a size-dependent statistical behaviour.

Keywords: Ductility; Thin films; Aluminium; Strain hardening

The ductility of thin metallic films is an important property in a variety of microsystems and coating applications. In flexible electronic devices, stretchability is essential for preserving electrical conductivity under large mechanical distortions [1–3]. In thin functional coatings, the material layer must be sufficiently ductile to sustain forming operations performed after deposition or to resist scratching or thermal loadings [4]. Micro- or nanoelectromechanical devices often involve thin metallic films that are either freestanding or lying on the substrate, and which might undergo moderate straining during operation or manufacturing [5,6]. In microelectronic devices, large strains in interconnects can result from severe thermal cycling and associated internal stress evolution [7]. In all these applications, a limited permanent deformation is sometimes tolerated, but without the occurrence of plastic localization or damage, in order to preserve the desired function.

Ductility is the capacity for a material to deform without cracking. Two main mechanisms limit the ductility of metals. The first is the occurrence of plastic localization by geometric necking or material instability. The strain corresponding to the onset of plastic localization is denoted here as ε_u. The second mechanism limiting the ductility is the accumulation of damage by nucleation, growth and coalescence of microvoids or microcracks. This paper essentially focuses on the resistance to plastic localization of thin films. The term "ductility" is thus defined, in the present context, as the strain corresponding to the onset of necking, which is often smaller than the true fracture strain.

Ductility in thin metallic films is known to be weaker than in the bulk counterpart (see a selection of references in which the ductility of metallic films is typically smaller than a few percent [8–10]). A similar loss of ductility is observed in bulk nanostructured materials (e.g. [11]). Similar to bulk nanocrystalline metals, thin films involve small grain sizes, but other specific phenomena related to the dominant presence of the surface are expected to play a major role. Indeed, some or even most of the dislocations can escape from the film (depending on the morphology and number of grains over the thickness, and on the presence of a possible surface oxide layer), thus limiting the strain-hardening capacity. Furthermore, it is important to remember that imperfections significantly affect the ductility of plastically deforming solids [12] and that the magnitude of typical

* Corresponding author. Address: Bâtiment Réaumur, Place Sainte Barbe 2, 1348 Louvain-la-Neuve, Belgium; e-mail: michael.coulombier@uclouvain.be

1359-6462/$ - see front matter © 2010 Acta Materialia Inc. Published by Elsevier Ltd. All rights reserved.
doi:10.1016/j.scriptamat.2010.01.048

imperfections can be expected to be larger in thin films compared to macroscopic samples. In the literature there are also examples of thin metallic film systems involving large ductility, associated, for instance, with high rate sensitivity triggered by grain growth mechanisms [13,14] or due to delocalization effects resulting from the presence of a soft underlying substrate [1–3].

In this paper, the resistance to plastic localization of freestanding Al films with thicknesses of 200 and 375 nm is investigated experimentally using a novel dedicated lab-on-chip tensile testing technique. The analysis focuses primarily on the observed wide scatter in the ductility, which is dependent on the specimen size and thickness, a topic which has not received any attention in the literature to date.

The tests were performed using a novel internal stress-driven lab-on-chip mechanical testing technique described in detail elsewhere [15]. The fabrication process involves the deposition of three layers on top of a silicon wafer. The first layer is a 1 μm thick silicon dioxide film deposited by plasma-enhanced chemical vapour deposition. This film acts as a sacrificial layer. The second layer is a 250 nm thick silicon nitride film deposited at 800 °C by low-pressure chemical vapour deposition, which provides approximately 1 GPa of internal stress. The high level of stress essentially comes from the thermal expansion mismatch between the silicon wafer and the silicon nitride. The third layer is made of a 200 or 375 nm thick film of pure Al deposited by e-beam evaporation; the grain size was measured on cross-sections by transmission electron microscopy (TEM) and was equal to ~150 and ~200 nm, respectively. The silicon nitride and aluminium layers are patterned by photolithography (see Fig. 1a and Ref. [15]). Dissolution of the underlying sacrificial layer is performed with 73% concentrated fluorohydric acid (HF), in order to release the two other layers from the substrate. The high tensile internal stress present in the second film, called the actuator, can now relax and, owing to its contraction, leads to deformation of the third film, called the specimen. Note that the deformation is occurring in the presence of HF and hence, in principle, without any oxide on the surface of the specimen (which is important regarding the potential effect of the surface oxide to act as a barrier to dislocation motion with an impact on the hardening behaviour). The contraction of the actuator imposes a displacement u on the Al specimen. The stress and strain in the test specimen can be determined from the measurement of u, as explained hereafter. Several samples are needed to generate a full stress–strain curve up to large strains. Large or small strains are obtained using long or short actuator lengths and short or long specimens, respectively. In the current design, the total length of the test structure (specimen and actuator) is equal to 0.5, 1, 1.5 or 2 mm, with different width ratios between the actuator and the specimen, i.e. 15/10, 15/8, 15/6, 15/4, 15/2, 15/1, 10/8, 10/6, 10/4, 10/2 and 10/1 (in μm).

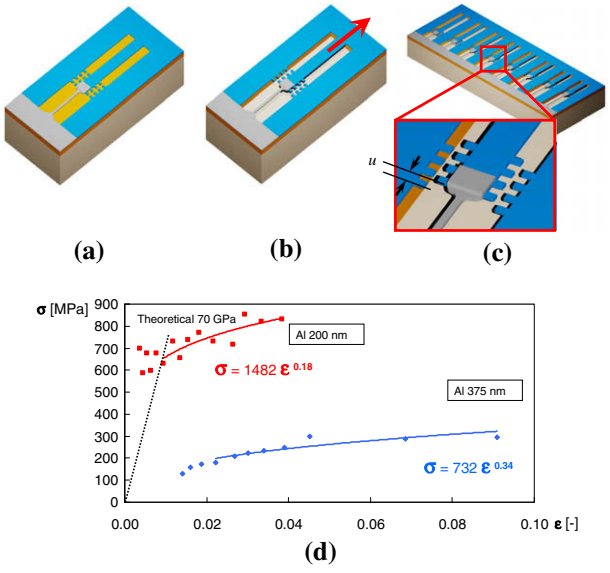

Figure 1. Suite of self-actuated tensile testing stages: (a) elementary tensile testing stage before release; (b) after release; (c) suite of tensile stages; and (d) true stress–true strain curves for 200 and 375 nm thick Al films.

The determination of the strain in the test specimen requires accurate measurement of u as well as of the dimensions and internal stress in the test material. As shown in Figure 1a–c, cursors have been designed on all test structures. The displacement u between the moving and fixed cursors is measured by scanning electron microscopy. Several cursors are introduced in order to repeat the measurements and improve the accuracy. The total strain in the specimen is the sum of the mechanical strain, ε^{mech}, and the mismatch strain, ε^{mis},

$$\varepsilon^{total} = \varepsilon^{mech} + \varepsilon^{mis} = \ln\left(\frac{L_0 + u}{L_0}\right) \tag{1}$$

where L_0 is the initial length of the specimen. The length L_0 is imposed by the design of the mask used for the photolithography, which has an error of less than 0.5 μm. The length of the specimens being always larger than several tens of micrometers, this error is negligible. The repeated measurements of u at high magnification lead to an absolute error of less than 50 nm. The mismatch strain ε^{mis} is the most difficult parameter to measure accurately. Many types of standard test structures [15–18] have been integrated in the lab-on-chip to cross-check the mismatch strain values. In the present Al films, the internal stress is very small (only a few MPa) and the mismatch strain is thus ignored, i.e. $\varepsilon^{mis} = 0$. The relative total error on the strain is smaller than 5% for the longest specimens and decreases with increasing deformation to reach values below 1–2% for the specimens reaching fracture (i.e. specimens reaching strains larger than typically 0.02–0.03 and sometimes much larger; see further below). The stress in each specimen can be calculated, based on load equilibrium, as (see Ref. [15] for details)

$$\sigma = E_a \frac{S_a}{S}\left(-\varepsilon_a^{mis} - \ln\left(\frac{L_{a0} + u}{L_{a0}}\right)\right) \tag{2}$$

where E_a is Young's modulus of the actuator material, S_a and S are the cross-section areas of the actuator and specimen, respectively, ε_a^{mis} is the mismatch strain of the actuator, measured with the same techniques as for ε^{mis}, and L_{a0} is the initial length of the actuator. The extraction of the stress is subjected to larger errors than for the strain. The error analysis regarding σ, which

is not a central quantity for the present study, is discussed elsewhere [15].

Plastic localization is observed in specimens deformed to sufficiently large strains. When plastic localization sets in, the extra overall displacement required to reach failure is small. Hence, due to the discrete nature of the test technique, specimens most often either fail or deform uniformly. Nevertheless, specimens with necking can sometimes be observed, such as in Figure 2 for 200 nm thick, 4 μm wide Al specimens. Figure 2a shows a diffuse necking process over a length scaling with the specimen width. At larger strains, a more localized necking mechanism develops that resembles a shear band oriented at about 55° from the main loading direction (see Fig. 2b and c). Finally, Figure 2c shows that damage develops within the shear band, leading to final fracture.

A qualitative observation of the test structures shows that the ductility is subjected to wide variations. For instance, in a series of specimens, one failed specimen followed by one nonfailed specimen is sometimes observed, even though the latter involves a larger strain. Furthermore, a series of shorter test structures systematically show larger ductility compared to longer test structures. In order to rationalize these observations, Figure 3 gathers the strain experienced by each tensile stage as a function of the specimen surface area for thicknesses equal to (a) 200 nm and (b) 375 nm, respectively. The failed specimens are indicated with open symbols.

In order to provide an accurate estimate of the strain that was applied to the failed specimens, it was assumed that the applied stress is equal to the stress experienced by the first nonfailed specimen located in the same series of structures. The displacement of the failed specimen as if no fracture had occurred is then obtained using Eq. (2). In some structures, fracture occurs at the overlap between the actuator and the specimen due to the local stress concentration and not in the gauge section of the dogbone specimen. Those samples are discarded. Finally, for some specimens, fracture is not caused by the deformation imposed by the actuator but is due to processing problems, such as a defect in the photoresist or dust particle on the wafer. In such instances, the failed samples are also not taken into account.

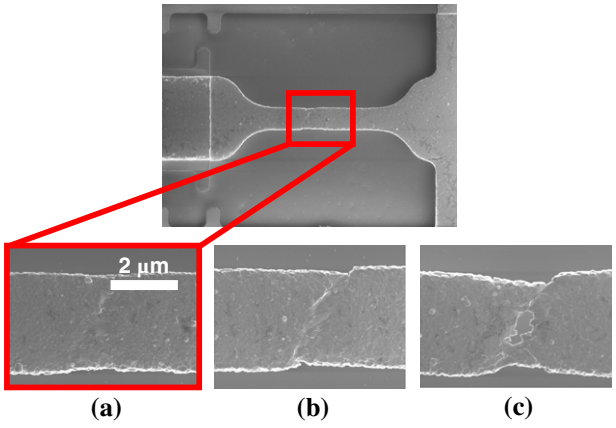

Figure 2. Plastic localization evolution observed in consecutive specimens with different strains involving (a) diffuse necking, (b) localized shear band process and (c) damage up to final failure.

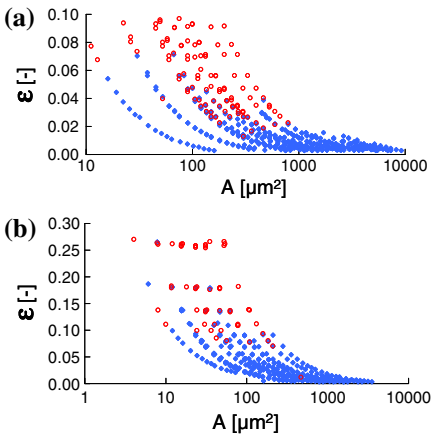

Figure 3. Strain as a function of the specimen surface area for (a) 200 nm thick and (b) 375 nm thick Al specimens. Open symbols indicate failed specimens, filled symbols indicate nonfailed specimens.

The strain-hardening exponent n has been extracted from eight and five stress–strain curves coming from eight and five different series of tensile stages for the 200 and 375 nm thick films, respectively, using Hollomon's law:

$$\sigma = K\varepsilon^n \tag{3}$$

where K is a hardening parameter. The mean strain-hardening exponent is equal to 0.11 ± 0.05 and 0.23 ± 0.12 for the 200 and 375 nm thick Al films, respectively.

In order to analyse more quantitatively the effect of the specimen size on ductility, the data of Figure 3 are converted in the form of a probability graph, as shown in Figure 4a. Because the technique involves a wide range of sample sizes and imposed strains, the data are grouped in different intervals of surface area and strain. For each interval, the probability of failure is calculated as the number of failed samples divided by the total number of samples within the same interval.

Figure 4b and c shows a statistical behaviour similar to the one observed for brittle materials, usually rationalized using Weibull-type analysis [19]. A maximum strain value is observed beyond which fracture occurs for all specimens. The maximum values are about 0.08 and 0.27 for the smallest specimens, made of 200 and 375 nm thick films, respectively. These values are not far from the average strain-hardening exponents n, estimated as 0.11 and 0.23, respectively. This implies that the Considère criterion, i.e. necking in rate-independent plastically deforming solids with no imperfection starts when $\varepsilon = n$, is approximately fulfilled for these specimens.

The fact that the Considère criterion is relatively well verified for small specimens means that the rate sensitivity of the Al films under investigation is probably small, otherwise a much larger uniform elongation would have been measured [12–14]. The main reason for the smaller ductility in the thinnest films is first related to the larger yield strength. A simple translation of the hardening curve, as a result of the Hall–Petch effect, directly implies a lower n, hence a lower uniform elongation. Differences in the strain-hardening behaviour are also possible between the two film thicknesses. First, the thinnest film, which involves a larger grain size to thick-

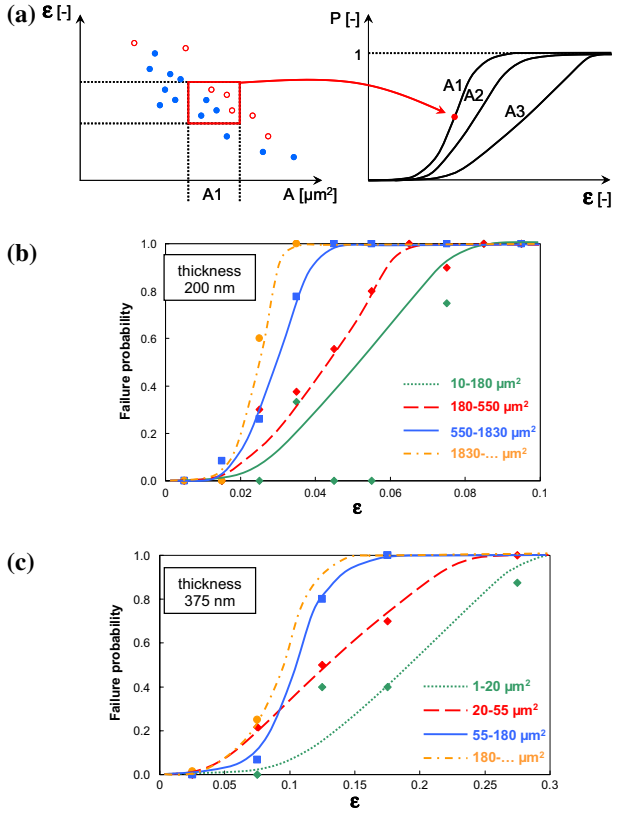

Figure 4. (a) Methodology for converting a "strain–surface" plot into a "probability of failure" graph; (b) probability of failure for the 200 nm thick and (c) for the 375 nm thick Al film.

ness ratio, will show a larger tendency for dislocation starvation. Furthermore, as the stress level is higher in the thinnest film, grain boundary relaxation effects, involving dislocation transmission or re-emission and accompanying decrease of the back stress, can provide additional reasons for a lower ductility [20,21]. These effects have not been investigated here.

The distribution of ductility shown in Figure 4 is explained by the presence of imperfections within the specimens. Imperfections are inherent to the fabrication process as a result of local thickness reduction due to the natural roughness, heterogeneities in the etching process or grain boundary grooving, or local width reduction due to the definition of the photoresist or material imperfection (e.g. a cluster of grains with weak orientations; see Ref. [23]). There is an increasing probability of producing larger imperfections when the surface area increases, as well as when the thickness decreases. The effect of imperfection on necking has been addressed by Hutchinson and Neale [12], who demonstrated that plastic localization is triggered earlier in the presence of imperfections. Recent computational studies based on strain gradient plasticity theory have addressed the same issue, showing that strain gradient effects can delay the necking process in micron-sized samples [22]. A model similar to the Weibull analysis of brittle failure in the framework of fracture mechanics is under development, based on size-dependent plastic localization theory.

As a conclusion, the ductility of thin evaporated Al films is strongly dependent on the thickness and on the surface area of the test specimen as a result of statistical distribution of imperfections. Large imperfections are more likely in specimens with larger surface area. The maximum ductility measured on the smallest specimens is equal to about 0.08 for 200 nm thick film and about 0.27 for 375 nm thick film, not far from the average strain-hardening exponents of 0.11 and 0.23, respectively, in agreement with the Considère criterion. The on-chip internal stress-actuated suite of tensile testing stages has proved to be a suitable tool with which to investigate the ductility of thin films with high-throughput capability.

The support of the Communauté Française de Belgique and of the Université catholique de Louvain through an ARC project, of MEMS Instruments for the development of the lab-on-chip technology, of the Fonds Belge pour la Recherche dans l'Industrie et l'Agriculture (FRIA) for M.C. and of the Belgian Science Policy through the IAP 6/24 project are gratefully acknowledged.

[1] S. Lacour, S. Wagner, Z. Huang, Z. Suo, Appl. Phys. Lett. 82 (2003) 2404.
[2] Y. Sun, J.A. Rogers, Adv. Mater. 19 (2007) 1897.
[3] S. Béfahy, S. Yunus, M. Troosters, T. Pardoen, P. Bertrand, Appl. Phys. Lett. 91 (2007) 141911.
[4] A.G. Evans, J.W. Hutchinson, Acta Mater. 43 (1995) 2507.
[5] S.M. Spearing, Acta Mater. 48 (2000) 179.
[6] F. Iker, N. Andre, T. Pardoen, J.-P. Raskin, J. Microelectromech. Syst. 15 (2006) 1687.
[7] Z. Suo, Comprehensive Structural Integrity, Elsevier, Amsterdam, 2007, p. 265 (Chapter 8.08).
[8] H.D. Espinosa, B.C. Prorok, B. Peng, J. Mech. Phys. Solids 52 (2004) 667.
[9] T. Tsuchiya, M. Hirata, N. Chiba, R. Udo, Y. Yoshitomi, T. Ando, K. Sato, K. Takashima, Y. Higo, Y. Saotome, H. Ogawa, K. Ozaki, J. Microelectromech. Syst. 14 (2005) 903.
[10] M.A. Haque, M.T.A. Saif, Acta Mater. 51 (2003) 3053.
[11] M.A. Meyers, A. Mishra, D.J. Benson, Prog. Mater. Science 51 (2006) 427.
[12] J.W. Hutchinson, K.W. Neale, Acta Metall. 25 (1977) 839.
[13] D.S. Gianola, D.H. Warner, J.F. Molinari, K.J. Hemker, Scripta Mater 55 (2006) 649.
[14] M. Legros, D.S. Gianola, K.J. Hemker, Acta Mater 56 (2008) 3380.
[15] S. Gravier, M. Coulombier, A. Safi, N. André, A. Boé, J.P. Raskin, T. Pardoen, J. Microelectromech. Syst. 18 (2009) 555.
[16] H. Guckel, D. Burns, C. Rutigliano, E. Lovell, B. Choi, J. Micromech. Microeng. 2 (1992) 86.
[17] J. Laconte, F. Iker, S. Jorez, N. André, J. Proost, T. Pardoen, D. Flandre, J.-P. Raskin, Microelectron. Eng. 76 (2004) 219.
[18] A. Boé, A. Safi, M. Coulombier, T. Pardoen, J.-P. Raskin, Thin Solid Films 518 (2009) 260.
[19] B.R. Lawn, T.R. Wilshaw, Fracture of Brittle Solids, Cambridge University Press, Cambridge, 1993.
[20] C.W. Sinclair, W.J. Poole, Y. Bréchet, Scripta Mater 55 (2006) 739.
[21] M. Delincé, P.J. Jacques, Y. Bréchet, J.D. Embury, M.G.D. Geers, T. Pardoen, Acta Mater 55 (2007) 2337.
[22] C.F. Niordson, V. Tvergaard, Int. J. Solids Struct. 42 (2005) 2559.
[23] M.G.D. Geers, W.A.M. Brekelmans, P.J.M. Janssen, Int. J. of Solids Struct. 43 (2006) 7304.